Electronic correlations in Fe at Earth's inner core conditions: Effects of alloying with Ni

O. Yu. Vekilova,[1,2] L. V. Pourovskii,[3,4] I. A. Abrikosov,[1,5] and S. I. Simak[1]

[1]*Department of Physics, Chemistry and Biology, Linköping University, SE-58183 Linköping, Sweden*

[2]*Multiscale Materials Modelling, Department of Materials and Engineering, Royal Institute of Technology (KTH), S-100 44 Stockholm, Sweden*

[3]*Centre de Physique Théorique, Centre national de la recherche scientifique, École Polytechnique, 91128, Palaiseau, France*

[4]*Swedish e-science Research Center, Department of Physics, Chemistry and Biology (IFM), Linköping University, Linköping, Sweden*

[5]*Materials Modeling and Development Laboratory, National University of Science and Technology (MISiS), Moscow, Russia*

(Received 22 July 2013; revised manuscript received 22 April 2015; published 8 June 2015)

We have studied the body-centered cubic (bcc), face-centered cubic (fcc), and hexagonal close-packed (hcp) phases of Fe alloyed with 25 at.% of Ni at Earth's core conditions using an *ab initio* local density approximation + dynamical mean-field theory approach. The alloys have been modeled by ordered crystal structures based on the bcc, fcc, and hcp unit cells with the minimum possible cell size allowing for the proper composition. Our calculations demonstrate that the strength of electronic correlations on the Fe 3*d* shell is highly sensitive to the phase and local environment. In the bcc phase, the 3*d* electrons at the Fe site with Fe only nearest neighbors remain rather strongly correlated, even at extreme pressure-temperature conditions, with the local and uniform magnetic susceptibility exhibiting a Curie-Weiss-like temperature evolution and the quasiparticle lifetime Γ featuring a non-Fermi-liquid temperature dependence. In contrast, for the corresponding Fe site in the hcp phase, we predict a weakly correlated Fermi-liquid state with a temperature-independent local susceptibility and a quadratic temperature dependence of Γ. The iron sites with nickel atoms in the local environment exhibit behavior in the range between those two extreme cases, with the strength of correlations gradually increasing along the hcp-fcc-bcc sequence. Further, the intersite magnetic interactions in the bcc and hcp phases are also strongly affected by the presence of Ni nearest neighbors. The sensitivity to the local environment is related to modifications of the Fe partial density of states due to mixing with Ni 3*d* states.

DOI: 10.1103/PhysRevB.91.245116 PACS number(s): 71.20.Be, 71.27.+a, 75.50.Bb, 91.60.Gf

I. INTRODUCTION

Iron is the main component of Earth's inner core. From geochemical and seismic data, it is generally assumed that iron in the Earth's core is alloyed with 10–15 at.% of Ni [1–2]. The pressure and temperature inside the inner core are estimated to be ∼330–364 GPa and ∼6000 K, respectively. They are too extreme to be easily accessible in modern diamond anvil-cell experiments, so the actual crystal structure is still a matter of debate. From the discovery of the Earth's core, the hexagonal close-packed (hcp) structure has been the primary candidate. However, in the past decade, a number of scientists started to advocate the body-centered cubic (bcc) Fe phase to be a suitable candidate for Earth's inner core material [3–4]. The bcc phase of Fe with 10 at.% of Ni has indeed been discovered experimentally at pressures and temperatures slightly lower than those of Earth's core [5], though this is still the only experimental indication of the existence of a high-temperature high-pressure bcc phase of Fe.

Despite a vast number of publications, most theoretical papers dedicated to the crystal structure and properties of Earth's core presumed Fe to be a nonmagnetic metal with insignificant electronic correlations [3–4,6–7]. This picture can be justified by noticing that high pressure and high temperature, when considered separately, are both expected to suppress the correlations and, hence, to destroy the magnetism in Fe. Under high pressure, the local Coulomb repulsion between the localized states (U) decreases due to the screening, while the bandwidth of these states (W) increases. The substantial reduction of the U/W ratio should lead to a decrease in the correlations' strength, thus justifying the use of standard mean-field approaches like the local density approximation (LDA) for the high-pressure studies. In addition, local magnetic moments are expected to be destroyed at high temperature by Stoner excitations.

Nevertheless, even the combined effect of extremely high pressure and temperature typical of Earth's core may not be sufficient to suppress significant electronic correlations in paramagnetic Fe. Pourovskii *et al.* [8] have recently shown that the pure bcc iron features a Curie-Weiss magnetic susceptibility and a non-Fermi-liquid behavior of the quasiparticle lifetime when local correlations are treated beyond the static mean-field level using dynamical mean-field theory (DMFT), while fcc and hcp Fe exhibit Fermi-liquid-like behavior. Ruban *et al.* [9] have predicted the existence of local magnetic moments of similar magnitude in all three (bcc, fcc, and hcp) phases of pure iron at Earth's core conditions using a longitudinal-fluctuation classical-spin model derived from disordered-local-moment density functional theory calculations.

However, as has been noticed in Ref. [10], the presence of Ni in Earth's core, often neglected in first-principles studies, may be important for understanding the physical properties of the system. For example, the tendencies toward relative stability of the bcc and hcp phases under pressure in pure iron and iron alloyed with nickel are the opposite of each other [10]. Motivated by recent papers in this area, we have studied the influence of Ni on electronic correlations in Fe-rich Fe-Ni alloys under the conditions of Earth's inner core. We have employed an *ab initio* LDA + DMFT approach to calculate the electronic structure of the bcc, fcc, and hcp phases for temperatures up to 5800 K and for densities corresponding to Earth's inner core. In the

calculations, we have used the volume equal to 7.05 Å/atom for all the considered phases. This volume corresponds to the estimated density of Earth's inner core, 13 155 kg/m^3, according to the Preliminary reference Earth model (PREM) [11].

We have made no attempt to match the experimentally reasonable Ni content (10–15 at.%) as well as the disordered state of Fe-Ni alloys expected under such extreme conditions [12]. They would require modeling with supercells, which are currently prohibitively large for *ab initio* DMFT calculations. Instead, we have considered small Fe_3Ni supercells (25 at.% of Ni) for all three phases. Despite their small sizes, these ordered structures provided us with two types of the local environment for Fe atoms in the case of the bcc and hcp lattices, with and without Ni in the first coordination shell of Fe. Therefore, with this choice of supercells, we have also been able to assess the impact of the local environment on electronic correlations between iron 3*d* states.

II. METHODS

The calculations have been carried out using a self-consistent in the charge density approach [13–14] combining the full-potential linearized augmented plane wave (FLAPW) WIEN2K [15] band structure method with a DMFT [16] treatment of the on-site Coulomb repulsion between the 3*d* states. The LDA+DMFT technique has previously been implemented to study the mechanical stability and magnetic properties of Fe [17–18].

For the on-site electron repulsion on Fe, we have employed the parameters $U = 3.40$ eV and $J = 0.90$ eV in all the considered phases, following the evaluations in Ref. [8] based on the constrained random phase approximation (cRPA) method [19–20], with the resulting Coulomb interaction matrices generated using the standard parameterization for the Slater integrals $U = F^0$, $J = (F^2 + F^4)/14$, and $F^2/F^4 = 0.625$ [21]. In Ref. [8], the U value has been found to be quite similar in the different phases of Fe, varying from 3.04 eV for the fcc to the 3.37 eV for the hcp crystal structures. Our test calculations of the dependence of the magnetic susceptibility and quasiparticle lifetime on the values of U for the Fe_3Ni system showed that the small differences in U (about 10%) did not induce any qualitative change in our results (see Figs. 1 and 2, and Figs. 11–13 in the Appendix). Some quantitative changes appeared when U on Fe was taken differently from U on Ni (3.4 eV on Fe and 2.75 eV on Ni, respectively). However, the typical dependence, i.e., the linear behavior with respect to temperature, remained unchanged. We also notice that those small differences may stem from a disentanglement procedure employed within cRPA, which is an approximation. Here, U on Fe may also be affected by doping with Ni. Due to all those uncertainties, we believe it is reasonable to neglect small differences in the value of U between the phases. Hence, we fixed U to the largest value obtained for the pure Fe phases, i.e., we took 3.4 eV for all the considered phases. For Ni in Fe_3Ni, we chose the same value as for Fe, which can be considered as an upper bound for the magnitude of U there. The calculated value of U in pure Ni is smaller than in Fe [22]; however, nickel sites in Fe_3Ni have a very different environment compared to that of pure Ni. Hence, no additional effects of correlations can be expected for Ni beyond those discussed below.

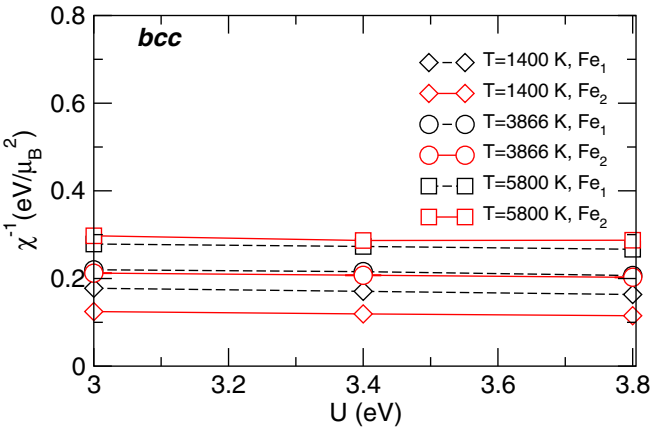

FIG. 1. (Color online) The dependence of the inverse uniform magnetic susceptibility on the values of U, varying from 3 to 3.8 eV for different temperatures in the bcc phase of Fe_3Ni. The solid red lines correspond to the Fe_2 type of Fe atoms; the dashed black lines correspond to the Fe_1 type. Diamonds, circles, and squares are used for the temperatures 1400, 3866, and 5800 K, respectively. As one may see, nearly horizontal lines mean that the increasing or decreasing of U by 10% does not quantitatively affect the results independent of the local environment around the Fe atoms (for both Fe_1 and Fe_2 types of atoms; the details on the atomic arrangement are described in Sec. II).

More details of the calculations can be found in Ref. [8]. The DMFT quantum impurity problem has been solved using the continuous time quantum Monte-Carlo (CT-QMC) method [23] as implemented in the TRIQS package [24], using 5×10^8 CT-QMC moves with the measurements performed after every 200 moves. For the Coulomb repulsion parameter, we have used the density-density Slater parameterization.

The uniform magnetic susceptibility has been computed as the reaction of the system to a small magnetic field applied

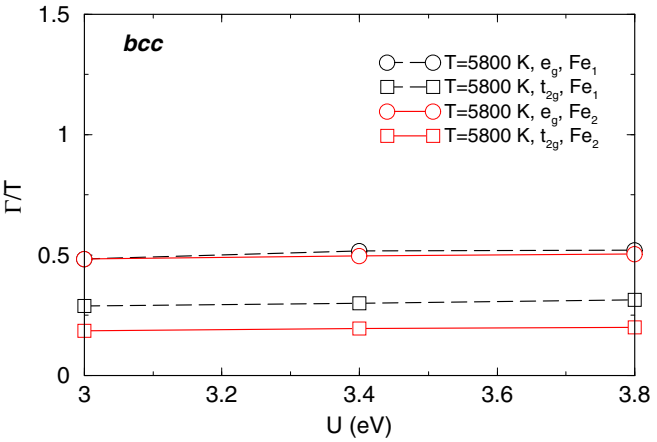

FIG. 2. (Color online) The dependence of the quasiparticle lifetime on the value of U for the temperature 5800 K in the Fe_3Ni bcc phase. The solid red lines correspond to the Fe_2 type of Fe atoms; the dashed black lines correspond to the Fe_1 type. Circles and squares are used for e_g and t_{2g}, respectively. As one may see, increasing or decreasing the value of U by 10% does not quantitatively change the results independent of the local environment around the Fe atoms.

on all sites. This susceptibility might be calculated for each site from the resulting on-site magnetic moment. The uniform magnetic susceptibility consists of the response to the field at a given site (i.e., its local susceptibility) as well as of the interaction with the moments induced by the same field on other sites. An external magnetic field of $H = 0.005$ eV/μ_B along the $\hat{z}$ axis has been added to the one-electron Hamiltonian in order to compute the uniform magnetic susceptibility $\chi = \frac{M}{H}$ from the resulting small magnetic moment M.

The static local susceptibility is a reaction of the system to a magnetic field applied to a given site only. This local susceptibility has been calculated via the spin-spin correlation function (computed during the CT-QMC calculations), to which it is related by the fluctuation-dissipation theorem [25]. The local magnetic susceptibility $\chi_{\rm loc} = \int_0^{1/T} \chi(\tau) d\tau$ has been computed from the imaginary-time on-site spin-spin correlation function $\chi(\tau) = \langle \hat{S}_Z(\tau)\hat{S}_Z(0)\rangle$ sampled by the CT-QMC method. Hence, by comparing the local and uniform susceptibilities of a given site, one may extract the magnitude of its exchange interaction with its neighbors.

In order to calculate the quasiparticle lifetime, the imaginary part of self-energy Σ for the first several frequencies has been fitted with a third degree polynomial and extrapolated to the zero frequency (see Fig. 3). The derivative has been taken in order to calculate $Z_{\rm eff}$ (the effective mass) at zero frequency. The imaginary-frequency self-energy has been analytically continued to the real axis using a stochastic maximum-entropy approach [26].

We used the standard double counting for metals, i.e., weakly correlated systems, the around mean-field expression [27]. As shown in Ref. [14], the LDA + DMFT electronic structure exhibits rather weak dependence on the choice of the double counting when the self-consistency in the charge density is included. $1 \times 1 \times 2$ bcc- and hcp-based cubic and hexagonal unit cells with three Fe atoms and one Ni atom have been used to simulate bcc and hcp Fe-Ni alloys, respectively. The c/a ratio for the hcp phase has been equal to 1.6 [28]. Also, the $L1_2$ structure with three Fe atoms and one Ni atom has been used to simulate fcc Fe-Ni alloy. Accordingly, there are two nonequivalent Fe atoms in the case of the bcc and hcp phases due to the differences in the local environment. Further, the Fe_1 type corresponds to the iron atom whose nearest neighbors are four (six) iron and four (six) nickel atoms in the bcc (hcp) structure, respectively. The second iron atom of the Fe_2 type is surrounded by exclusively iron atoms in the first coordination shell. For the fcc cell, all three Fe atoms are equivalent, so one deals only with the case where the local environment of Fe atoms contains Ni.

III. RESULTS

The temperature evolution of the LDA + DMFT inverse magnetic susceptibility has been calculated for temperatures in the range from 1000 to 5800 K and is shown in Fig. 4. In the case of the bcc phase [Fig. 4(b)], the inverse magnetic susceptibility of the Fe_2 type (red solid line) exhibits strong and linear temperature dependence. This behavior can be described by the Curie-Weiss law and hints at the presence of a local magnetic moment on this site. This result is in good agreement with Ref. [8], where a Curie-Weiss temperature evolution has

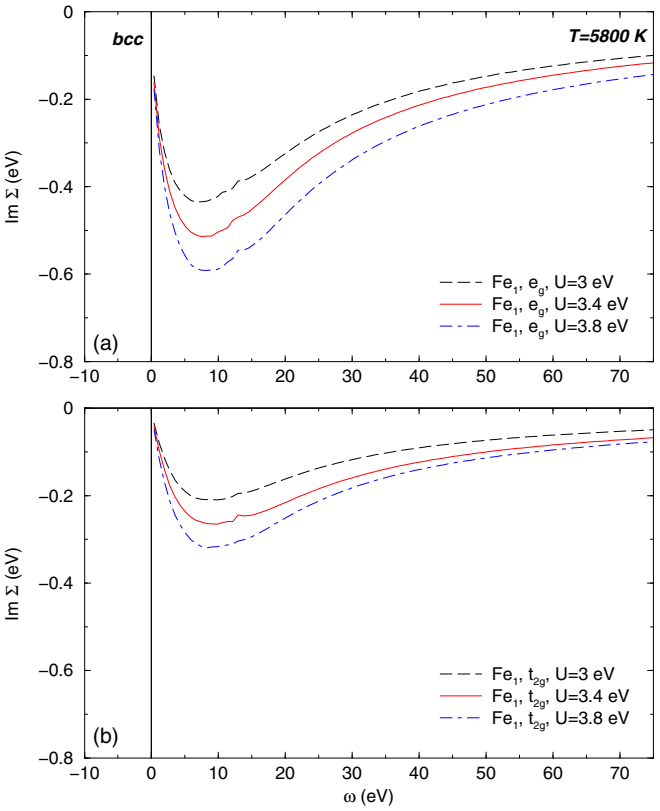

FIG. 3. (Color online) The dependence of the imaginary part of self-energy on the frequency for different values of U for the bcc phase of Fe_3Ni: (a) e_g and (b) t_{2g} states. Temperature is equal to 5800 K. Black dashed, red solid, and blue dashed-dotted lines correspond to the U values of 3, 3.4, and 3.8 eV, respectively. As one may see, all three curves are close to each other at low frequencies, meaning that the corresponding values for the mass enhancement and inverse quasiparticle lifetime exhibit a rather weak dependence on variations of U within this range.

been obtained for pure bcc iron. Hence, the Fe_2 atoms that have only Fe nearest neighbors exhibit magnetic properties similar to those of pure bcc iron. In contrast, the inverse magnetic susceptibility of the Fe_1 atoms (black dashed line) shows a weaker and nonlinear temperature dependence, which can be expected for a Pauli paramagnet at high temperature. This difference points to a significant reduction in electronic correlations on Fe sites that have Ni nearest neighbors.

The magnetic susceptibility of Ni itself is small and exhibits rather weak temperature dependence (see Fig. 5). Similar LDA + DMFT calculations have been carried out for the hcp and fcc phases of Fe_3Ni [Figs. 4(a) and 4(b), respectively], and nonlinear and rather weak temperature dependence of the magnetic susceptibility has been obtained. The magnetic susceptibility of Ni sites (Fig. 5) in those phases exhibits a similar temperature evolution. Total uniform magnetic susceptibility for all the considered phases is presented in Fig. 6.

The inverse of magnetic susceptibility of the Fe_2 atoms in the bcc phase has been fitted to the Curie-Weiss law

$$\frac{1}{\chi} = \frac{3\,(T+\Theta)}{\mu_{\rm eff}^2}. \qquad (1)$$

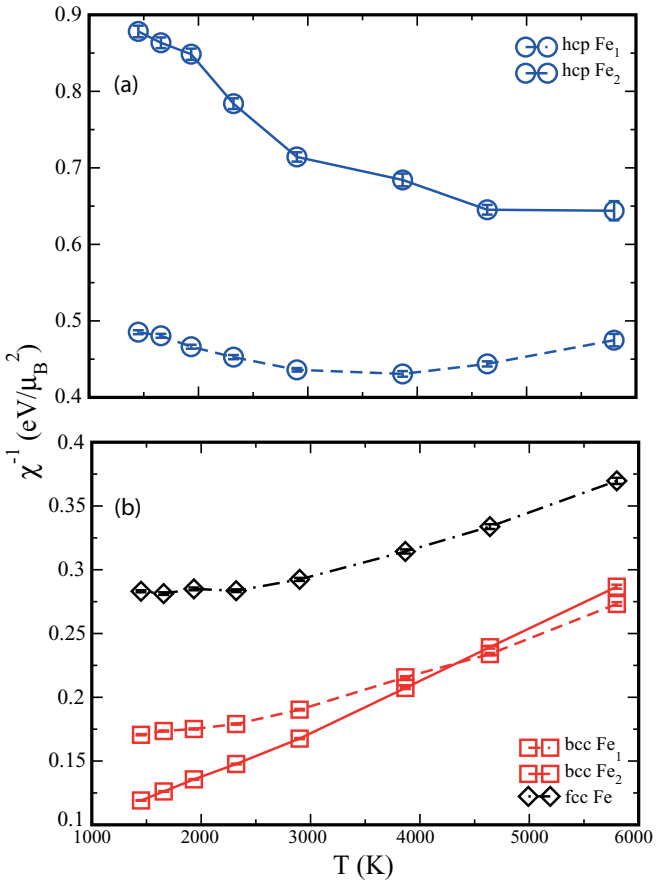

FIG. 4. (Color online) (a) The inverse uniform magnetic susceptibility in the paramagnetic state as a function of temperature for the hcp phase, with the dashed and solid lines corresponding to the Fe_1 (six Ni and six Fe nearest neighbors) and the Fe_2 (all nearest neighbors are Fe) types, respectively. The error bars show the stochastic CT-QMC error. (b) The same data for the bcc and fcc phases of the Fe_3Ni alloy. Dashed red line corresponds to the Fe_1 type of iron atoms, whose nearest neighbors are four Fe and four Ni atoms in the bcc structure. The solid red line shows the Fe_2 type of atoms, which are surrounded exclusively by Fe atoms. The dashed-dotted black line shows the Fe atoms of the fcc phase. The error bars show the stochastic CT-QMC error.

The calculated effective local magnetic moment μ_{eff}, at the volume corresponding to the pressure ~300 GPa is 2.6 μ_B and $\Theta = 1347$ K. The parameter Θ here comprises two terms: a characteristic coherence temperature, around which a crossover from the correlated high-temperature state to a low-temperature Fermi-liquid one takes place [29], and a contribution from intersite magnetic interactions (see, e.g., Ref. [16]).

In order to extract the contribution of intersite interactions to the uniform susceptibility, we have also calculated the imaginary-time spin-spin correlation functions and evaluated the corresponding static local magnetic susceptibilities (i.e., response functions to a static on-site magnetic field) χ_{loc}. In the spirit of effective Hamiltonian approaches, we assume that one can define an effective spin Hamiltonian of the system comprising a sum of on-site terms, which encode the response to a local static field, and intersite interactions. With these assumptions and within a static mean-field theory, the local

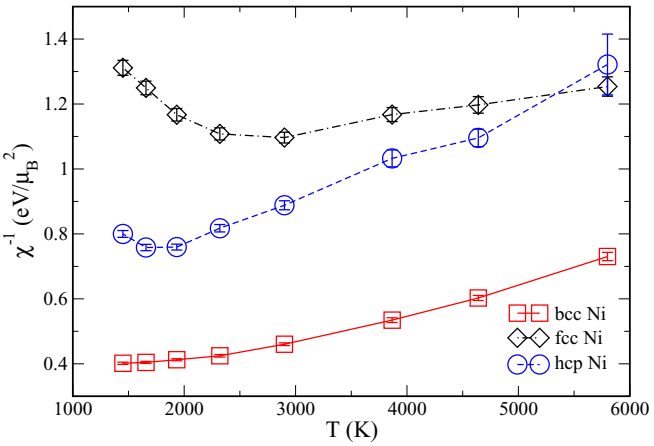

FIG. 5. (Color online) The inverse uniform magnetic susceptibility of the paramagnetic state as a function of temperature for the Ni atom in the bcc, fcc, and hcp phases of the Fe_3Ni alloy. The solid red line corresponds to the Ni atoms in the bcc structure of the Fe_3Ni alloy; the dashed-dotted black line shows the Ni atoms in the fcc structure; and the blue dashed line corresponds to the Ni atoms in the hcp structure. The error bars show the stochastic CT-QMC error.

and uniform susceptibilities for a given site are related as

$$\chi^{(-1)}(\omega = 0) = \chi_{\text{loc}}^{-1}(\omega = 0) - J_0, \tag{2}$$

where J_0 is the sum of all intersite exchange interactions of this site with the other sites.

Calculated inverse χ_{loc} of Fe sites vs temperature is shown in Fig. 7(a). One may notice that the local susceptibility of Fe is very sensitive to the phase and local environment. It is virtually temperature independent for the Fe_2 type of the hcp phase, the behavior characteristic for a weakly correlated itinerant Fermi liquid. A linear temperature evolution of $1/\chi_{\text{loc}}$ for the Fe_2 site in bcc Fe_3Ni is expected for correlated systems with local moments. Here, χ_{loc} of other Fe types are

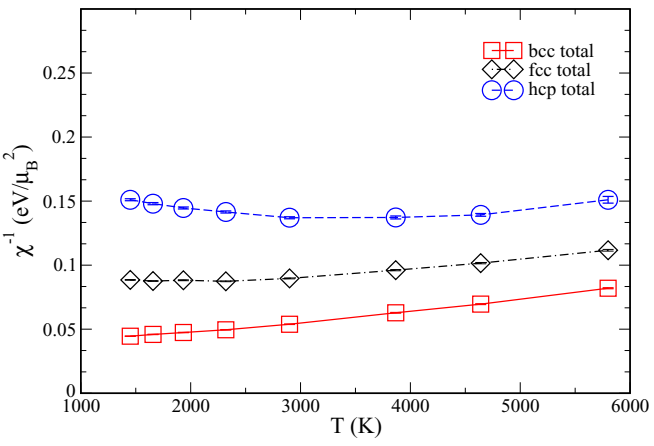

FIG. 6. (Color online) The inverse total uniform magnetic susceptibility of the paramagnetic state as a function of temperature for the Ni atom in the bcc, fcc, and hcp phases of the Fe_3Ni alloy. The solid red, dashed-dotted black, and dashed blue lines correspond to the total magnetic susceptibility of the bcc, fcc, and hcp structures of the Fe_3Ni alloy, respectively. The error bars show the stochastic CT-QMC error.

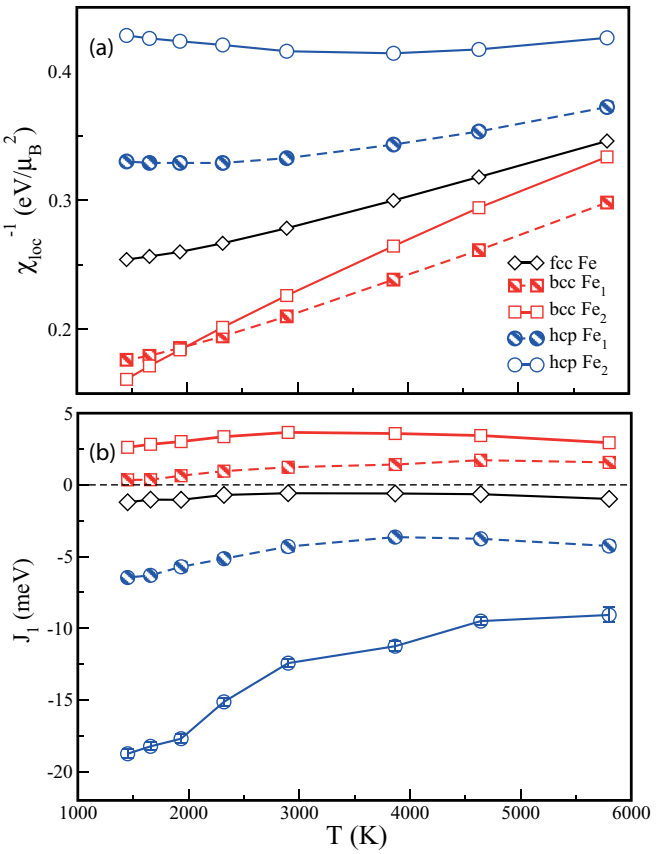

FIG. 7. (Color online) (a) The inverse local susceptibility of Fe atoms in the bcc, fcc, and hcp Fe_3Ni phases vs temperature. The notation for iron sites (Fe_1, Fe_2) is the same as in Fig. 1. (b) The average intersite nearest-neighbor exchange interaction as function of temperature. The positive/negative values correspond to ferromagnetic/antiferromagnetic interactions, respectively.

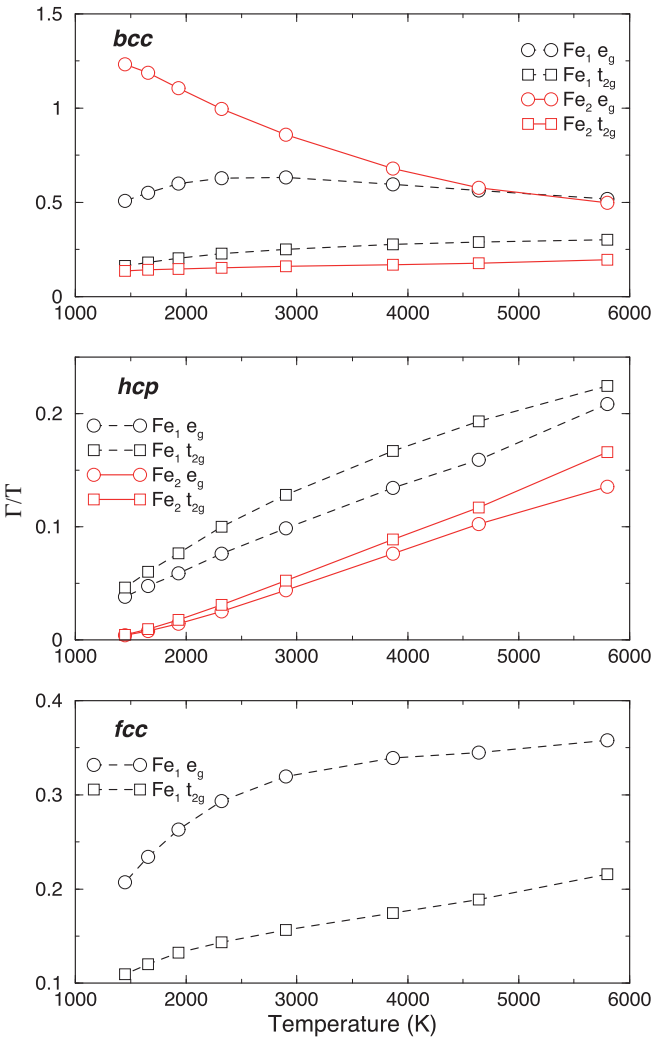

FIG. 8. (Color online) The ratio of the inverse quasiparticle lifetime Γ to temperature T vs T for the bcc, fcc, and hcp phases of the Fe_3Ni alloy. The dashed black lines correspond to e_g (circles) and t_{2g} (squares) of the Fe_1 type. The solid red lines correspond to e_g and t_{2g} of the Fe_2 type, respectively.

in between those two extremes: inverse local susceptibilities of the Fe_1 site in bcc and Fe in fcc feature clear deviations from linearity, while $\chi_{\rm loc}$ of the Fe_1 site in hcp exhibits a moderate decrease with temperature.

From this analysis, we conclude that the qualitative difference in temperature evolution of the uniform susceptibilities is mainly due to on-site correlations captured by $\chi_{\rm loc}$, in contrast to the results of Ref. [9]. However, the contribution of the intersite interactions to the actual magnitude of uniform susceptibility is also significant, as one may notice by comparing corresponding χ and $\chi_{\rm loc}$. We have evaluated J_0 using Eq. (2) and then have extracted the average nearest-neighbor intersite interaction J_1 assuming that longer range interactions are negligible (this assumption is not very reasonable for the weakly correlated itinerant fcc and hcp phases; however, we plot the intersite interactions in this form to allow for a simpler comparison with the data on J_1 obtained by other methods). Then $J_0 = 2\sum_i J_{0i} \sim 2zJ_1$, where i runs over the nearest neighbors of a given site 0, z is the coordination number equal to 12 and 8 for fcc/hcp and bcc, respectively.

The resulting interaction J_1 vs temperature is plotted in Fig. 7(b). Here, J_1 favors ferromagnetic ordering in the bcc phase and antiferromagnetic in the fcc and hcp phases, in agreement with the well-known tendencies of the corresponding pure Fe phases at lower pressure-temperatures. One may expect that a large and rather strongly temperature-dependent J_1 for Fe_2 in the hcp phase in fact comprises significant contributions from longer range antiferromagnetic interactions, making this system highly frustrated. One may also notice that the presence of Ni nearest neighbors leads to drastic reduction of intersite correlations in both the bcc and hcp phases.

We have also evaluated the strength of correlations in all three phases by analyzing the low-frequency behavior of the DMFT self-energy. The degree of non-Fermi-liquid behavior can be estimated from the inverse quasiparticle lifetime, which reads

$$\Gamma = -Z\,\mathrm{Im}[\Sigma(i0^+)] \tag{3}$$

where the quasiparticle residue Z is calculated as

$$Z^{-1} = 1 - \left.\frac{\partial \mathrm{Im}\sum(i\omega)}{\partial\omega}\right|_{\omega\to 0^+}, \tag{4}$$

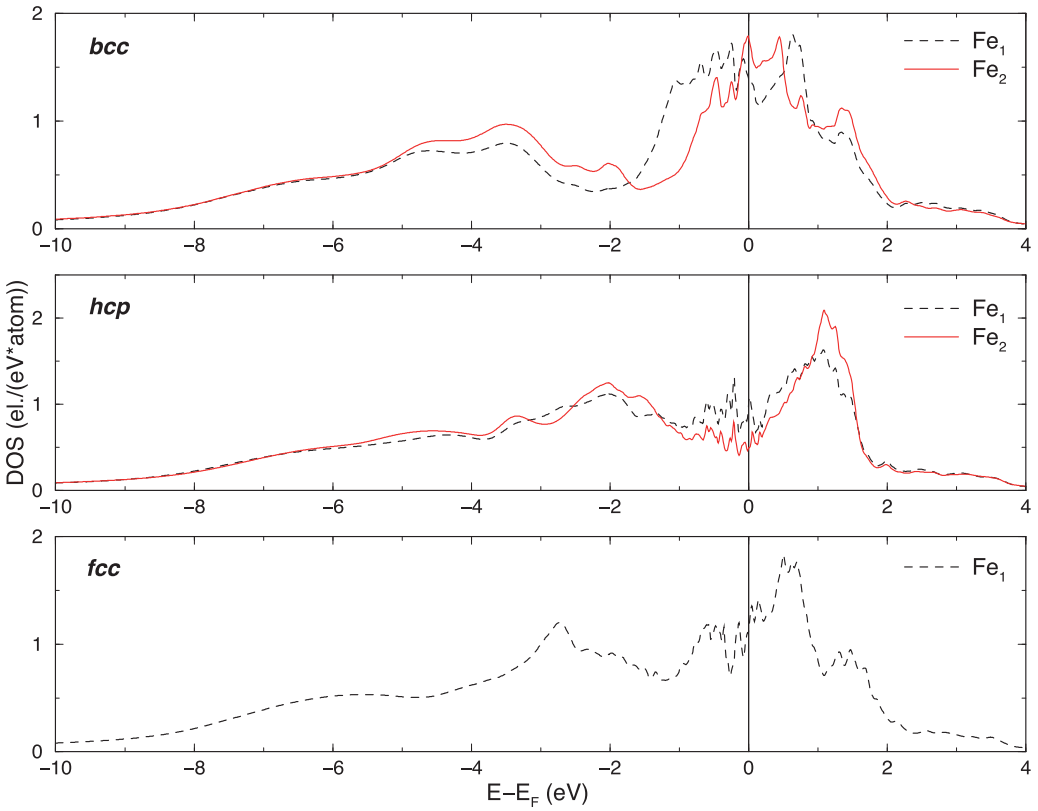

FIG. 9. (Color online) The LDA + DMFT partial DOS of iron for the bcc, fcc, and hcp phases of the Fe_3Ni alloy. The dashed black and solid red lines are the partial DOS of the Fe_1 type and Fe_2 types, respectively.

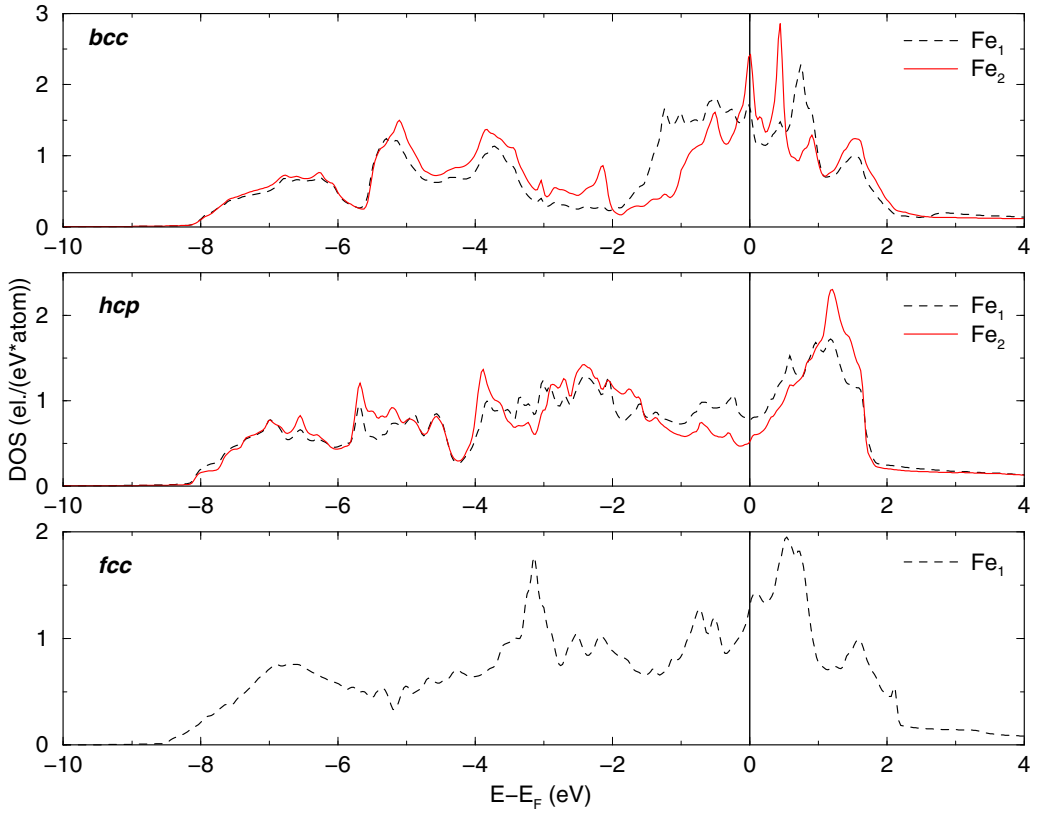

FIG. 10. (Color online) The LDA partial DOS of iron for the bcc, fcc, and hcp phases of the Fe_3Ni alloy. The dashed black and solid red lines are the partial DOS of the Fe_1 type and Fe_2 types, respectively.

from the imaginary-frequency self-energy $\Sigma(i\omega)$ extrapolated to zero. Here, ω stands for the frequency.

The temperature evolution of the inverse quasiparticle lifetime Γ/T for the relevant irreducible representations of the Fe $3d$ shell of all three phases is shown in Fig. 8.

In the Fermi-liquid regime, the inverse quasiparticle lifetime scales as T^2 and, therefore, a linear dependence of Γ/T vs temperature is expected. In the bcc phase, the e_g states of Fe_1 (dashed black line) and Fe_2 (solid red line) behave in a quite different way. At high temperatures (higher than 1000 K), Γ/T of the Fe_2 atoms exhibits substantial deviations from linearity and decreases with temperature, indicating the noncoherent nature of these states. We note that the presence of a local magnetic moment at the Fe_2 site inferred from the Curie-Weiss temperature dependence of its magnetic susceptibility is consistent with this manifestly non-Fermi-liquid behavior of the corresponding quasiparticle lifetime. As discussed in Ref. [8], the Curie-Weiss-like behavior of magnetic susceptibility can also be explained within a Fermi-liquid picture as being due to the large peak at the Fermi energy in the density of states (DOS) of the bcc phase. However, such an explanation cannot simultaneously account for the non-Fermi-liquid temperature dependence of the quasiparticle lifetime. Γ/T of the Fe_1 atoms for the e_g states increases with temperature up to around 2400 K, and the deviations from the linear regime begin at higher temperatures. This behavior is intermediate between the strongly nonlinear e_g states of Fe_1 and the quasilinear dependence observed for weakly correlated states, e.g., for bcc t_{2g}. The t_{2g} states of both Fe_1 and Fe_2 in the bcc phase, as well as the e_g states of the fcc Fe, show rather small deviations from the linear regime and thus from the Fermi-liquid behavior. In the hcp phase, the behavior of Γ/T vs temperature is almost perfectly linear for all Fe sites and representations, as expected for a Fermi liquid.

In Figs. 9 and 10, we display the partial DOS (PDOS) of Fe and Ni in all three Fe_3Ni phases obtained within LDA + DMFT and LDA, respectively.

By comparing the corresponding LDA and LDA + DMFT PDOS, one may observe a noticeable quasiparticle renormalization in bcc and fcc, while the hcp PDOS is almost unaffected by correlations. A prominent peak is present at the Fermi level E_F of the LDA Fe PDOS of bcc Fe_3Ni. The width of this peak at half-maximum differs in the Fe_1 and Fe_2 cases, with the Fe_2 peak being significantly narrower. A narrow peak at E_F is associated with rather strong correlations in bcc Fe, as has been previously discussed in Refs. [8,30–31]. Thus, the d electrons of Fe_1 become less correlated due to the effect of Ni nearest neighbors, which induce a broadening of the peak at E_F, while the overall d band bandwidths remain similar in both Fe_1 and Fe_2.

IV. CONCLUSIONS

We have carried out a theoretical study of the role of electronic correlations in the Fe_3Ni alloy at pressures ~300 GPa and temperatures up to 5800 K, corresponding to Earth's inner core conditions within an *ab initio* LDA + DMFT approach.

Our calculations have demonstrated strong sensitivity of electronic correlations and the iron magnetism in Fe_3Ni to the phase and local environment. In the bcc phase, the Fe sites with exclusively Fe nearest neighbors feature a Curie-Weiss uniform susceptibility corresponding to a local magnetic moment of 2.6 μ_B, while the Fe sites with four Ni nearest neighbors exhibit a weakly temperature-dependent Pauli-like susceptibility. The temperature evolution of the local susceptibility is also strongly affected by the phase and environment. It ranges from a strong inverse temperature dependence observed in the bcc phase for the Fe sites with Fe-only nearest neighbors to an almost constant Pauli-like behavior for the corresponding Fe sites in hcp. The intersite exchange interactions are ferromagnetic in bcc and antiferromagnetic in hcp and fcc. In the bcc and hcp, they are strongly affected by the presence of Ni nearest neighbors. A similar sensitivity to the phase and local environment has been observed for the quasiparticle lifetime in the bcc phase, with the overall picture being in perfect agreement with the one inferred from the analysis of the magnetic susceptibility. The sensitivity to the local environment is explained by the broadening of the Fe partial DOS at the Fermi level due to mixing with itinerant states of its Ni neighbors, which remain weakly correlated. Correspondingly, in real iron-rich Fe-Ni bcc alloys, if they are stable at the inner core Earth conditions, one may expect strong variations in the correlations' strength between different Fe sites due to variations in the local environment. As in the case of pure iron [8], the Fe_3Ni fcc and hcp phases behave as rather weakly correlated Fermi liquids; however, the intersite antiferromagnetic correlations in hcp are also significantly affected by the local environment.

ACKNOWLEDGMENTS

We are thankful to HPC-Europa2 for support of this project. L. V. Pourovskii gratefully acknowledges the financial support of the Ministry of Education and Science of the Russian Federation in the framework of Increase Competitiveness Program of NUST "MISiS" (No. K3-2015-038); travel support provided by PHD DALEN under Project No. 26228RM. Support from the Swedish Research Council (VR) Projects No. 621-2011-4426, No. 2011-42-59, and No. 2014-4750; Linköping Linnaeus Initiative for Novel Functional Materials (LiLi-NFM); the Swedish Foundation for Strategic Research (SSF) program SRL10-0026; the Swedish Government Strategic Research Area Grant in Materials Science "Advanced Functional Materials" (AFM); and the Swedish e-Science Research Centre (SeRC) are gratefully acknowledged. I. A. Abrikosov acknowledges the support from the Grant of the Ministry of Education and Science of the Russian Federation (Grant No. 14.Y26.31.0005). The computations were partly performed on resources provided by the Swedish National Infrastructure for Computing (SNIC).

APPENDIX

In this Appendix we present our results concerning the dependence of the uniform and local susceptibility (Figs. 11 and 12, respectively) as well as the inverse quasi-particle lifetime (Fig. 13) on the value of the Coulomb repulsion U. As one sees, while varying the value of U does induce some quantitative changes, it does not affect the qualitative evolution of the susceptibilities or quasi-particle lifetime as function of temperature.

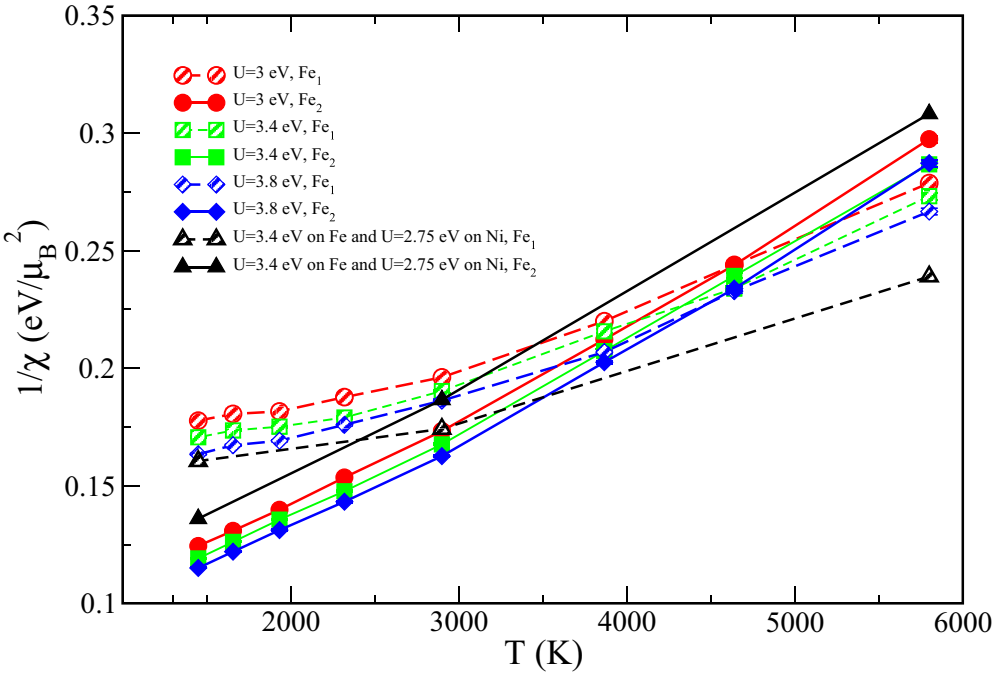

FIG. 11. (Color online) The dependence of the inverse uniform magnetic susceptibility on temperature for different values of U in the bcc phase of Fe_3Ni. The solid and dashed lines correspond to the Fe_2 and Fe_1 types of Fe atoms, respectively. Red circles, green squares, and blue diamonds are used for the U values 3, 3.4, and 3.8 eV, respectively. Black triangles are used for the U value on Fe atoms equal to 3.4 eV and U on Ni atoms equal to 2.75 eV. As one may see, the dependence of the susceptibility on temperature during the increasing or decreasing of U by 10% does not quantitatively affect the results independent of the local environment around the Fe atoms. As one may also see, when U on Fe is equal to 3.4 eV and U on Ni is equal to 2.75 eV, the qualitative dependence remains the same; i.e., the linear behavior of the inverse magnetic susceptibility of the Fe_2 type of atoms and nonlinear behavior on the Fe_1 type remained unchanged.

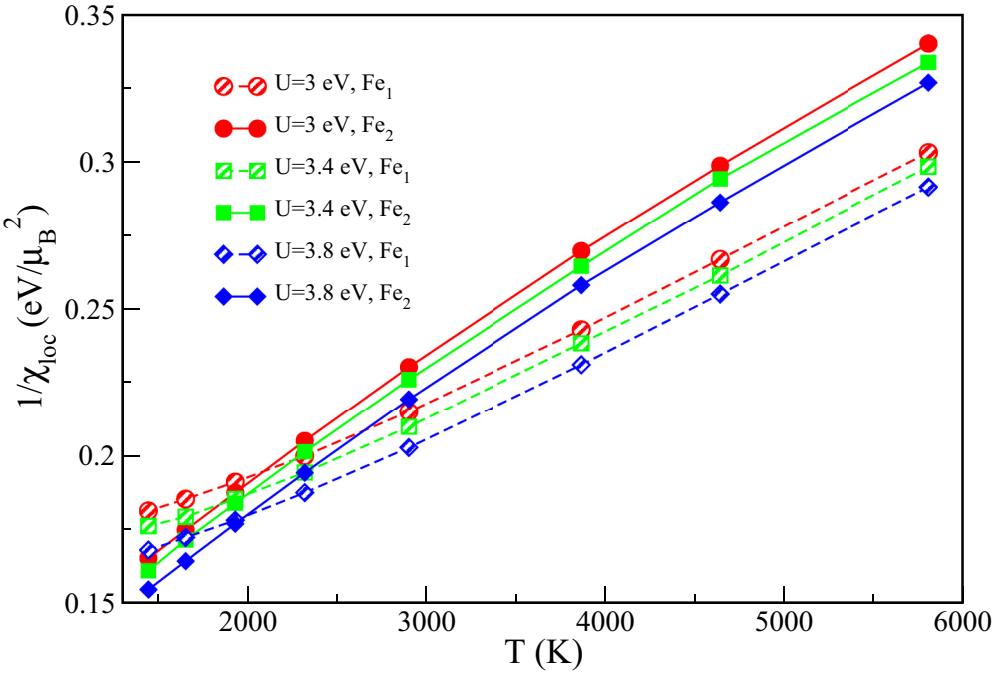

FIG. 12. (Color online) The dependence of the inverse local magnetic susceptibility on temperature for values of U, varying from 3 to 3.8 eV in the bcc phase of Fe_3Ni. The solid and dashed lines correspond to the Fe_2 and Fe_1 types of Fe atoms, respectively. Red circles, green squares, and blue diamonds are used for the U values 3, 3.4, and 3.8 eV, respectively. As one may see, the dependence of the susceptibility on temperature during the increasing or decreasing of U by 10% does not quantitatively affect the results independent of the local environment around the Fe atoms.

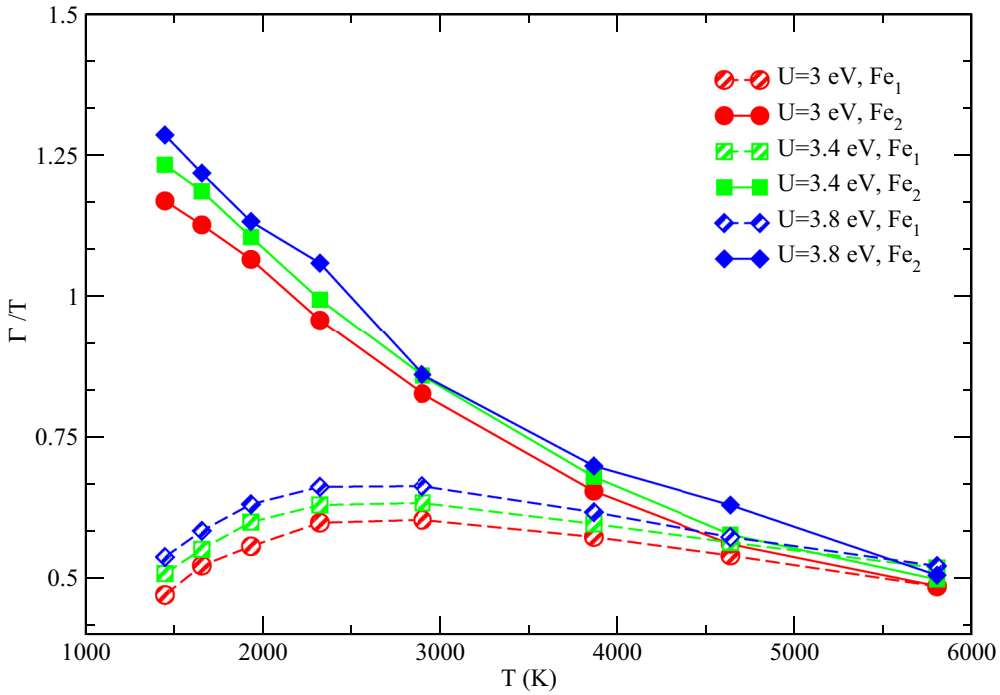

FIG. 13. (Color online) The dependence of the inverse quasiparticle lifetime Γ to temperature T vs T for values of U, varying from 3 to 3.8 eV in the bcc phase of Fe_3Ni. The solid and dashed lines correspond to the Fe_2 and Fe_1 types of Fe atoms, respectively. Red circles, green squares, and blue diamonds are used for the U values 3, 3.4, and 3.8 eV, respectively. As one may see, the dependence of Γ/T on temperature during the increasing or decreasing of U by 10% does not quantitatively affect the results independent of the local environment around the Fe atoms.

[1] F. Birch, J. Geophys. Res. **57**, 227 (1952).
[2] R. J. Hemley and H. K. Mao, Int. Geol. Rev. **43**, 1 (2001).
[3] A. B. Belonoshko, R. Ahuja, and B. Johansson, Nature **424**, 1032 (2003).
[4] L. Vocadlo, D. Alfe, M. J. Gillan, I. G. Wood, J. P. Brodholt, and G. D. Price, Nature **424**, 536 (2003).
[5] L. Dubrovinsky, N. Dubrovinskaia, O. Narygina, I. Kantor, A. Kuznetzov, V. B. Prakapenka, L. Vitos, B. Johansson, A. S. Mikhaylushkin, S. I. Simak, and I. A. Abrikosov, Science **316**, 1880 (2007).
[6] A. S. Mikhaylushkin, S. I. Simak, L. Dubrovinsky, N. Dubrovinskaia, B. Johansson, and I. A. Abrikosov, Phys. Rev. Lett. **99**, 165505-1 (2007).
[7] L. Stixrude, Phys. Rev. Lett. **108**, 055505 (2012).
[8] L. V. Pourovskii, T. Miyake, S. I. Simak, A. V. Ruban, L. Dubrovinsky, and I. A. Abrikosov, Phys. Rev. B **87**, 115130 (2013).
[9] A. V. Ruban, A. B. Belonoshko, and N. V. Skorodumova, Phys. Rev. B **87**, 014405 (2013).
[10] O. Yu. Vekilova, S. I. Simak, A. V. Ponomareva, and I. A. Abrikosov, Phys. Rev. B **86**, 224107 (2012).
[11] A. M. Dziewonski and D. L. Anderson, Phys. Earth Planet. Inter. **25**, 297 (1981).
[12] M. Ekholm, A. S. Mikhaylushkin, S. I. Simak, B. Johansson, and I. A. Abrikosov, Earth Planet. Sci. Lett. **308**, 90 (2011).
[13] M. Aichhorn, L. Pourovskii, V. Vildosola, M. Ferrero, O. Parcollet, T. Miyake, A. Georges, and S. Biermann, Phys. Rev. B **80**, 085101 (2009).
[14] M. Aichhorn, L. Pourovskii, and A. Georges, Phys. Rev. B **84**, 054529 (2011).
[15] P. Blaha, K. Schwarz, G. Madsen, D. Kvasnicka, and J. Luitz, *WIEN2k, An augmented Plane Wave + Local Orbitals Program for Calculating Crystal Properties* (Karlheinz Schwarz, Techn. Universität Wien, Austria, 2001).
[16] A. Georges, G. Kotliar, W. Krauth, and M. J. Rozenberg, Rev. Mod. Phys. **68**, 13 (1996).
[17] I. Leonov, A. I. Poteryaev, V. I. Anisimov, and D. Vollhardt, Phys. Rev. Lett. **106**, 106405 (2011).
[18] A. I. Lichtenstein, M. I. Katsnelson, and G. Kotliar, Phys. Rev. Lett. **87**, 067205 (2001).
[19] F. Aryasetiawan, M. Imada, A. Georges, G. Kotliar, S. Biermann, and A. I. Lichtenstein, Phys. Rev. B **70**, 195104 (2004).
[20] T. Miyake and F. Aryasetiawan, Phys. Rev. B **77**, 085122 (2008).
[21] V. I. Anisimov, F. Aryasetiawan, and A. I. Lichtenstein, J. Phys.: Condens. Matter **9**, 767 (1997).
[22] T. Miyake, F. Aryasetiawan, and M. Imada, Phys. Rev. B **80**, 155134 (2009).
[23] E. Gull, A. J. Millis, A. I. Lichtenstein, A. N. Rubtsov, M. Troyer, and P. Werner, Rev. Mod. Phys. **83**, 349 (2011).
[24] M. Ferrero and O. Parcollet, "TRIQS: A toolbox for research on Interacting Quantum Systems", http://ipht.cea.fr/triqs.

[25] See, e.g. G. D. Mahan, *Many-Particle Physics* (Kluwer Academic/Plenum Publishers, New York, 2000), pp. 174–177.
[26] K. S. D. Beach, arXiv:cond-mat/0403055.
[27] M. T. Czyżyk and G. A. Sawatzky, Phys. Rev. B **49**, 14211 (1994).
[28] S. Tateno, K. Hirose, Y. Ohishi, and Y. Tatsumi, Science **330**, 359 (2010).
[29] K. Haule and G. Kotliar, New J. Phys. **11**, 025021 (2009).
[30] R. Maglic, Phys. Rev. Lett. **31**, 546 (1973).
[31] V. Y. Irkhin, M. I. Katsnelson, and A. V. Trefilov, J. Phys.: Condens. Matter **5**, 8763 (1993).